Indonesian Journal of Electrical Engineering and Computer Science
Vol. 32, No. 1, October 2023, pp. 121~128
ISSN: 2502-4752, DOI: 10.11591/ijeecs.v32.i1.pp121-128

Using (Ba,Ca)ScO_2F:Bi^{3+},K^+ phosphor with great performance and strong heating stability for LED backlight screens

Le Doan Duy[1], My Hanh Nguyen Thi[2], Nguyen Le Thai[3]
[1]Faculty of Basic Sciences, Vinh Long University of Technology Education, Vinh Long Province, Vietnam
[2]Faculty of Mechanical Engineering, Industrial University of Ho Chi Minh City, Ho Chi Minh City, Vietnam
[3]Faculty of Engineering and Technology, Nguyen Tat Thanh University, Ho Chi Minh City, Vietnam

Article Info

Article history:

Received Sep 7, 2022
Revised Jul 14, 2023
Accepted Jul 15, 2023

Keywords:

Color homogeneity
Double-layer phosphor
Luminous flux
Monte Carlo theory
WLEDs

ABSTRACT

The current diodes emit illumination (LED) display study is focused on strait-band green phosphor samples yielding significant effectiveness as well as heating consistency. The cation substitution design technique was used to create $Ba_{1-x}Ca_xScO_2F$:0.001Bi^{3+},0.001K^+ with x of 0-0.12) perovskite phosphors that emit strait green illumination when activated by a 415 nm chip. The impact of Ca^{2+} replacement for Ba^{2+} in the crystal structures of $Ba_{1-x}Ca_xScO_2F$:0.001- Bi^{3+},0.001K^+ and photoluminescence characteristics were examined. In the space group *Pm3m*, all of the phosphors have a cubic perovskite-type structure. The development of cell characteristics and the lengthiness of the Ba/ Ca/K/Bi-O bonds were studied. Beneath 415 nm chip stimulation, the phosphors with an interior quantum effectiveness of 77.4 percent produce strong green radiation reaching the peak at 510 nm. The increase of luminous effectiveness and heating steadiness in response to local structural change was thoroughly addressed. The cation substitution design technique discussed here might be a significant way to realizing spectrum modulation by regulating the micro-surrounding within the latticework to achieve outstanding LED backlighting screens.

Corresponding Author:

My Hanh Nguyen Thi
Faculty of Mechanical Engineering, Industrial University of Ho Chi Minh City
No. 12 Nguyen Van Bao Street, Ho Chi Minh City, Vietnam
Email: nguyenthimyhanh@iuh.edu.vn

1. INTRODUCTION

Currently, phosphor-transformed diodes emit white illumination (pt-wLEDs) have garnered a lot of interest as potential technologies for backlight displays [1]–[3]. As new-generation solid-state illumination supplies, they outperform conventional lighting in terms of longevity, stability, energy efficiency, luminous efficacy, environmental protection, and other factors [4], [5]. The most common method of manufacturing w-LEDs for backlight displays involves a merger between one blue InGaN chip and YAG:Ce^{3+} phosphor along with nitride $(Sr,Ca)_2Si_5N_8$:Eu^{2+} red phosphor [6]–[8]. Nevertheless, these phosphors' ull width at half-maximum (FWHM) values are too big (over 100 nm and 90 nm, respectively), limiting their uses. Meanwhile, owing to the shortage of green radiation, the hue scale for the backlights would merely exceed ~80% national television standards committee (NTSC) criteria under the commission on illumination (CIE) 1931 concept [9], [10]. Nonetheless, the shortage of green radiation diminishes the vibrancy of the hues. As a result, it is critical to investigate an elevated-effectiveness strait band green emitting phosphor with exceptional heating steadiness. Various green emitting phosphors have been created to rise the hue gamut in order to suit the needs of backlighting technologies [11]. For instance, the green phosphors Sr_2SiO_4:Eu^{2+} (hue scale reaching 74.7 percent of the NTSC criteria), β-sialon:Eu^{2+} (hue gamut reaching 82.1 percent of the NTSC value) and

$SrGa_2S_4:Eu^{2+}$ (Color Gamut - 83.8 percent of the NTSC value) are combined with red emitting phosphor [12], [13]. It is worth mentioning that the constructed device's greatest color gamut is <90% of the NTSC criteria, a result that isn't too significant for the hue spectrum. The cation replacement method would be effective for creating phosphors with elevated-quality luminescence characteristics. The advantages range between red/blue shift adjustment for the emitting maximum location and increased illumination effectiveness or heating steadiness [14], [15]. The power transmission between Ce^{3+} and Mn^{2+} from $(Lu_{1-x}Y_x)_3Al_{4.8}Si_{0.2}O_{12}:0.1Ce^{3+},0.2Mn^{2+}$ garnet solid compound, for example, may be altered via replacing Lu^{3+} ions via Y^{3+}, being related to the decrease in the space separating the ions of Ce^{3+} as well as Mn^{2+} within the dodecahedron. The Ca/Ba substitution in the $Ba_2MgSi_2O_7:Eu^{2+}$ host can be used to move the emitting band to longer wavelengths by increasing the Eu^{2+} 5d electron crystal field cleavage [16], [17]. It is possible to adjust the valence line for the host latticework via substituting Sr^{2+} for Ba^{2+} within $Ba_2SiO_4:Eu^{2+}$ due to increased structural stiffness and improved heating radiation steadiness. In most situations, phosphors with optimum photoluminescence characteristics may be obtained by cation substitution design.

In this paper, we describe a phosphor with a maximal stimulation wavelength of 415 nm and a vivid green radiation. The $Ba_{1-x}Ca_xScO_2F:Bi^{3+},K^+$ (with x value of 0-0.12) compositions were created using the cation replacement technique, which began with $BaScO_2F:Bi^{3+},K^+$. By substituting smaller Ca^{2+} ions for larger Ba^{2+} ions, a sequence of $Ba_{1-x}Ca_xScO_2F:Bi^{3+},K^+$ (x = 0-0.12) phosphors were created. The structural development, morphology, absorbing spectra, luminous characteristics, temperature-dependent luminous characteristics, and LED backlight efficiency of these materials were all thoroughly examined. The impacts of microstructure modification on luminous strength augmentation, red shift for the emitting line, as well as heating steadiness enhancement were thoroughly examined. Furthermore, one w-LED product offering one great hue scale reaching 110% of the NTSC criteria was found utilizing the combined phosphor as a green emitter, indicating great potential implementation in backlighting displays.

2. METHOD

The solid-state reactivity under great heat level approach was used to create phosphor powders $Ba_{1-x}Ca_xScO_2F:0.001Bi^{3+},0.001K^+$ (x = 0, 0.03, 0.06, 0.09, and 0.12). Various pure substances acquired from Aladdin were blended $BaCO_3$, BaF_2, Sc_2O_3, $CaCO_3$, Bi_2O_3, as well as K_2CO_3. The blend was then calcinated in a box furnace at 1200ºC for 8 hours. The specimens were then subjected to calcination under 1100^0C for 4 hours within lowering aerosphere (H_2 10% + N_2 90%) gaseous combination for obtaining the three-valence status in Bi granules [18]. The resultant compounds were progressively chilled then coarsely pulverized to be further analyzed.

X-ray diffractometry was used to characterize the crystal layouts of the specimens utilizing X-ray diffractometry, using Cu-Kα radioactivity with cathode voltage and pipe current reaching 30 kilovolts and 20 milliamperes. The general structure analysis system (GSAS) software performed the structural improvements. Scanning electron microscopy (SEM) and energy dispersive spectrometry were used to characterize the micro-formations along with elemental compounds for the specimens. A UV-VIS-NIR spectrophotometer was used to measure the absorbing spectra of the specimens in the 200-800 nm range. The photoluminescent (PL) along with PL exciting spectra (PLE) were computed at room temperature utilizing a fluorescence spectrophotometer and a 150 W Xe lamp. One F-7000 accompanied by a Quanta-φ incorporated globular orb along with a polytetrafluoroethylene specimen dome was used to measure the internal quantum efficiencies. An FLS980 spectrometer accompanied by one Xe light under 450 W in the form of the stimulation supply was utilized to study the temperature-dependent luminescence parameters. One FLS920 spectrometer implemented onto one nanosecond flashing light to acquire a stimulation supply was used to measure the lifetimes. The integrating sphere approach was used to analyze the photoelectric characteristics for the produced WLED device, consisting of the PL spectra, hue coordination, along with color rendering index (CRI). A transparent silicone resin was mixed with $Ba_{0.94}Ca_{0.06}ScO_2F:0.001Bi^{3+},0.001K^+$ phosphor and commercial $CaAlSiN_3:Eu^{2+}$ phosphor to make the w-LEDs. After vacuuming out the bubbles, we daubed the resulting slurry above one 415-nm NUV chip then fired it under 100 ºC within 1 hour then 150 ºC within 3 hours.

3. RESULTS AND DISCUSSION

There are the XRD patterns for all $Ba_{1-x}Ca_xScO_2F:0.001Bi^{3+},0.001K^+$ powders (x = 0, 0.03, 0.06, 0.09, and 0.12). All diffraction peaks are clearly compatible with those of $BaScO_2F$, indicating pure phase formation. As a result of effectively acquiring the anticipated phosphors while co-doping Bi^{3+},K^+, and Ca^{2+}, the primary phase structure does not alter [19]. Because of the reduced ionic radius of Ca^{2+} (1.34 Å) replacing Ba^{3+} (1.61 Å), all the diffraction peaks shift to greater angles as the Ca^{2+} concentration rises. The Bragg equation might explain these shifts in XRD patterns [20]:

$$2d\ sin\theta = n\lambda \quad (1)$$

where d represents the interplanar distance, λ represents the X-ray wavelength. θ represents the diffraction angle. The Ba^{2+} granules would be substituted using tinier Ca^{2+} ions, causing the unit cellule as well as the gap to shrink. Rietveld rectifications for X-ray diffraction (XRD) behaviors would be done to study crystal structure disorder produced by Ca^{2+} doping. There are the improved crystallographic characteristics of $Ba_{1-x}Ca_xScO_2F:Bi^{3+},K^+$ with x values of 0, 0.03, 0.06, 0.09, and 0.12. The refinement's residual factors (R) focalize at an insignificant level, suggesting that the rectification findings can be deemed accurate. The cell characteristics as well as cell volume V reduce as the Ca^{2+} doping concentration increases. It is demonstrated that Ca^{2+} ion doping has a clear effect imposed on $(Ba/Ca/Bi/K)O_{12}$ polyhedron, shrinking alongside growing Ca^{2+} concentration, leading to the lesser binding spans d(Ba/Ca/Bi/K-O). As a result, variations in bond length (Bi-O) cause deformation of the $[BiO_{12}]$ polyhedra then alter the crystal field stability for Bi^{3+}. Slight displacements of polyhedra can result in asymmetric contracting, twisting, and bending kinds of polyhedra, leading to the varying states for polyhedral deformation. The asymmetric contraction for the (Bi-O) bonds is responsible for the deformation of the BiO_{12} polyhedra. As a result, the polyhedral deformation index (D) may be determined as:

$$D = \frac{1}{n}\sum_{i=1}^{n}\frac{|d_i - d_{av}|}{d_{av}} \quad (2)$$

d_i signifies the span among the centered particle and the i-th coordination particle. d_{av} signifies the mean span for a link. As is well known, increasing the polyhedral distortion of BiO_{12} can result in increased crystal field cleavage for Bi^{3+}, resulting in lesser $^1S_0$-$^3P_1$ power state shift. The crystal layout for $(Ba,Ca)ScO_2F$:0.001-Bi^{3+},0.001K^+ reveals that the unit cellule would include angle-bonded $[Sc(O/F)_6]$ accompanied by the Ba/Ca/Bi/K cation found under the octahedral cavity alongside cuboctahedral $[Ba/Ca/Bi/K(O/F)_{12}]$. The anion sublatticework would include transposed oxygen as well as fluorine within about 67:33 percent proportion. Based on the fault relation, the allowable percentage variation for the ion radius between the incorporated and alternative ions should remain below 25% to demonstrate the Ca^{2+} replacement relationship in the host. The following equation may be used to compute the replacement relationship [21]:

$$D_r = 100 \times \frac{[R_m(CN) - R_d(CN)]}{R_m(CN)} \quad (3)$$

D_r denotes the radius percent dissimilarity. R_m denotes the base cation radii. R_d demotes incorporated granule radii. CN denotes the coordinating values. As previously stated, the ion radius for incorporated Ca^{2+} (rCa^{2+} = 1.34Å, CN = 12) would be identical to that of Ba^{2+} (r Ba^{2+} = 1.61Å, CN = 12)[34], and the radius proportion disparity among Ba^{2+} and Ca^{2+} is 16.6%, which is less than the limitation amount. Ca^{2+} ions may thus be incorporated with the $BaScO_2F$ base for the task of substituting Ba^{2+} locations. In comparison to $BaScO_2F:Bi^{3+},K^+$, $Ba_{0.94}Ca_{0.06}ScO_2F$:-Bi^{3+},K^+ possesses comparatively high crystallinity. The Ba, Ca, Sc, O, F, Bi, and K factors are evenly dispersed across the $BaScO_2F$ motes, indicating that Ca^{2+}, Bi^{3+}, and K^+ would be effectively integrated with the crystal latticework. The PL stimulation and PL spectra of $Ba_{1-x}Ca_xScO_2F:Bi^{3+},K^+$ (x = 0, 0.03, 0.06, 0.09, and 0.12) were examined to evaluate the impact of Ca^{2+} substituting Ba^{2+} on the luminescence characteristics in the host. When x = 0.06 is used instead of x = 0, the maximal strength of radition is enhanced by 2.5 times. This is owing to the tiny particle magnitude for Ca^{2+} ions used as an alternative to larger atomic size Ba^{2+} ions. Because of the lattice shrinkage impact, which minimizes the non-radioactive alleviation then improves the stiffness for $BaScO_2F$ configuration frameworks, the luminous efficiency of the $Ba_{1-x}Ca_xScO_2F:Bi^{3+},K^+$ phosphors are increased. The photoluminescence intensity diminishes when a considerable amount of Ba^{2+} is replaced by Ca^{2+} owing to the creation for faulty power states. Inner quantum performances for $Ba_{1-x}Ca_xScO_2F:Bi^{3+},K^+$ (x = 0, 0.06) measured at room temperature reach 54.3 % and 77.4 %. As Ca^{2+} substitution for Ba^{2+} increases, the emitting bands illustrate a noticeable red shift from 504 to 510 nm. The red shift is caused by a decrease in cell volume (or latticework factors) along with crystal latticework diminution, which generally results in a severe crystal field splitting. As we are aware, a little change in the bond lengthiness for the Bi^{3+} coordination environment with an increase in Ca^{2+} concentration can cause a change in the Bi $^3P_1$ trajectorial cleavage, Stokes shift, as well as centroid shift. As a result, we must describe the alteration in the crystal field, calculated using an expression [22]:

$$D_q = \frac{Ze^2r^2}{6R^5} \quad (4)$$

D_q signifies the cleavage power. Z signifies the anion charge. e signifies the electron charge. r signifies the radius for d-wave function. R signifies the lengthiness of the bind regarding the luminous cation and its ligand.

According to the expression above, D_q would be mostly determined by R. The average bond length R decreases when Ba^{2+} ions are replaced with Ca^{2+} ions, resulting in more crystal field splitting. As a result, the red shift for the discharge line would be caused by an increase in the crystal splitting for Bi^{3+} ions Furthermore, the inclusion regarding doping ions reduces symmetry, which changes the favored orientation of a Bi^{3+} P orbital, as a result of which the Bi^{3+} emission changes into one greater wavelength. The phosphor degradation period is determined by the trigger's radiation as well as the non-radioactive shift mechanism. As a result, study of the decay curves can shed light on the luminescence decay kinetics. The degradation arches for the $Ba_{1-x}Ca_xScO_2F:Bi^{3+},K^+$ (with x values of 0, 0.03, 0.06, 0.09, and 0.12) specimens tracked under normal temperature. The double-exponential function can be used to approximate the decay curves [23]:

$$I(t) = I_0 + A_1 \exp\left(\frac{-t}{\tau_1}\right) + A_2 \exp\left(\frac{-t}{\tau_2}\right) \tag{5}$$

t denotes time. $I(t)$ signifies the luminous strength for that moment, A_1 and A_2 signifies the fitting constants. τ_1 and τ_2 the degradation durations correlating with the respective exponential elements. The median duration τ^* may be represented as [24].

$$\tau^* = \frac{A_1{\tau_1}^2 + A_2{\tau_2}^2}{A_1\tau_1 + A_2\tau_2} \tag{6}$$

The ground state for Bi^{3+} generated by the $6s^2$ electron arrangement would be widely known to be the $^1S_0$ state. Bi^{3+} statuses subjected to excitation having the 6s6p setting would be $^3P_0$, $^3P_1$, $^3P_2$, and $^1P_1$. Spin is absolutely banned during the shifts between $^1S_0$ and $^3P_0$ as well as $^3P_2$. Spin-orbit coupling mixes the two energy levels $^3P_1$ and $^1P_1$. As a result, only the $^1S_0 \rightarrow {}^3P_1$ along with $^1S_0 \rightarrow {}^1P_1$ transitions possess enough absorptivity power. Bi^{3+} luminescence is greatly influenced by the crystalline surrounding within the base latticework.

The temperature stability of the phosphors as produced has a significant impact on the implementations of elevated-quality wLEDs. As a result, the heating quenching behavior of the as-prepared phosphor must be evaluated. As the heat rises, the summed emission intensities of all the specimens decrease, increase, and then decrease. The shift of the population among the $^3P_0$ and $^3P_1$ stimulated states, as well as the ejection for electrons stuck within defects, result in increased emitting strengths under heat levels. Overall, the heat abatement was linked mostly to an increase of non-radioactive shift possibility. The increased thermal stability can be attributed to higher structural stiffness and increased defect development in the host. To assess the structural stiffness of Ca^{2+}-doped phosphors further, the Debye heat level regarding the particle with crystallography ($\Theta_{D,i}$) would be determined using anisotropic particle translocation factors utilizing the expression as [25]:

$$\Theta_{D,i} = \sqrt{\frac{3\hbar^2 T N_A}{A_i k_B U_{iso,i}}} \tag{7}$$

A_i signifies the particle mass. k_B signifies the Boltzmann constant. $\hbar$ signifies the Planck constant, $U_{iso,i}$ denotes the particle average translocation factor. $\Theta_{D,i}$ signifies reversely proportional to U_{iso}. Refinement yielded the U_{iso} values for $Ba_{1-x}Ca_xScO_2F:Bi^{3+},K^+$ (x = 0, 0.06). The findings demonstrate that $Ba_{0.94}Ca_{0.06}ScO_2F:Bi^{3+},K^+$ possesses an U_{iso} reaching 0.01042, which is the same as that of $BaScO_2F:Bi^{3+},K^+$ (0.01307). Based on the findings, $Ba_{0.94}Ca_{0.06}ScO_2F:Bi^{3+},K^+$ possess a higher stiffness than $BaScO_2F:Bi^{3+},K^+$, which is 0.4461), 4369 K correlated color temperature (CCT), and 27.00 lm W^{-1} luminance efficiency (LE). For the task of getting the LED's hue spectrum, white light was filtered using ordinary commercial color filters. To better understand the phosphor's chromatic characteristics, the chroma clarity was computed using as [26]:

$$Color\ purity = \frac{\sqrt{(x-x_i)^2+(y-y_i)^2}}{\sqrt{(x_d-x_i)^2+(y_d-y_i)^2}} \tag{8}$$

(x, y) is the coordination for sample $Ba_{0.94}Ca_{0.06}ScO_2F:Bi^{3+},K^+$. (x_i, y_i) is the hue coordination for equivalent-power white illumination shown as (0.3333, 0.3333). (x_d, y_d) is the coordination for the illuminant's correlated prevalent wavelength [27]. The computed hue purity of the sample is around 68.4%, which makes it suitable for use in backlight displays. Furthermore, the hue scale for WLED fabrication may achieve 110.3% level of the NTSC criteria. Based on the photoelectric properties, the sample is determined to be an effective green-element source. The LED offering the broad hue range as well as good hue fidelity demonstrated shows promise for use in backlight displays. Judging Figure 1, the $YAG:Ce^{3+}$ presence is inversely proportional to $(Ba,Ca)ScO_2F:Bi^{3+},K^+$. Said altreration leads to certain outcomes: one is to sustain median CCTs, and the other

is to influence how two phosphor layers within our WLED device assimilate then disperse illumination, altering the hue precision as well as illumination efficiency in the device. As such, the $(Ba,Ca)ScO_2F:Bi^{3+},K^+$ dosage results in the chroma standard in said device. The $YAG:Ce^{3+}$ dosage declined to maintain the mean CCTs while the $(Ba,Ca)ScO_2F:Bi^{3+},K^+$ dosage grew from 2% to 20% Wt. The same is relevant in the case of WLEDs, which have chroma temperature scope from 5600 K to 8500 K.

The effect of $(Ba,Ca)ScO_2F:Bi^{3+},K^+$ presence upon the transmittance spectrum of our device shall be clearly shown in Figure 2. We might be able to make a decision depending on the requirements of the manufacturer. High-hue-grade WLED devices might somewhat reduce lumen. White ray would be generated based on the spectral range, as seen via Figure 2. The temperatures shown by these five photos are 5600K, 6600K, 7000K, 7700K, as well as 8500K. Obviously, the intensity for specific spectrum zones (420-480 as well as 500-640 nm) escalates alongside $(Ba,Ca)ScO_2F:Bi^{3+},K^+$ dosage. Said extension for the dual-band discharge spectrum suggests a lumen extension. On the other hand, with the superior blue-illumination dispersion in the WLED device, the dual phosphor sheets will augment chroma consistency. Manipulating the chroma consistency for the phosphor setting at elevated heats could be challenging. The study shows that $(Ba,Ca)ScO_2F:Bi^{3+},K^+$ may boost the hue standard of WLEDs at both high and low hue heats (5600K and 8500K).

Thus, this dual-layer distant phosphor sheet's effectiveness at generating illuminating beam has been shown via the investigation. Figure 3 results, in particular, demonstrate that when $(Ba,Ca)ScO_2F:Bi^{3+},K^+$ concentration increased from 2 % weight to 20 % weight, a considerable increase in the luminous flux was also seen. Judging Figure 4, the phosphor $(Ba,Ca)ScO_2F:Bi^{3+},K^+$ concentration under every median CCT values greatly decreased the hue deviation. The red phosphor sheet's absorptivity can explain this. When the $(Ba,Ca)ScO_2F:Bi^{3+},K^+$ takes in the blue ray generated via the LED chip, the blue-phosphor motes change the blue ray into green one. Furthermore, these motes will assmilate yellow illumination as well. On the other hand, the LED chip's blue illumination can assimlate a greater amount of blue glow, surpassing other absorptivity demonstrated owing to the material's absorption strengths. Subsequently, $(Ba,Ca)ScO_2F:Bi^{3+},K^+$ increases the amount of green illumination for the WLED device, boosting hue uniformity. Hue consistency would be a paramount factor in for WLED lights. WLED cost escalates under greater chroma consistency. On the other hand, $(Ba,Ca)ScO_2F:Bi^{3+},K^+$ would not be costly, hence may become broadly applicable.

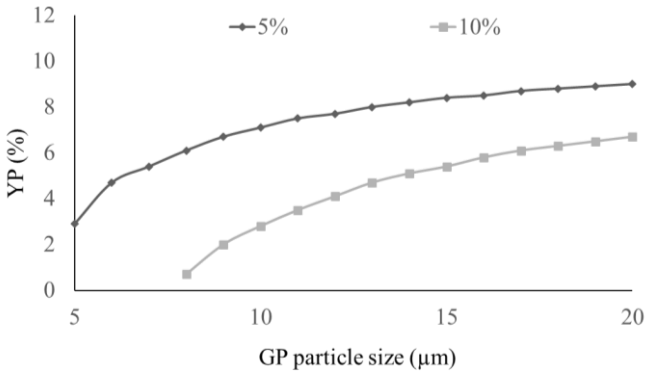

Figure 1. Altering phosphor dosage, thus maintaining mean CCT

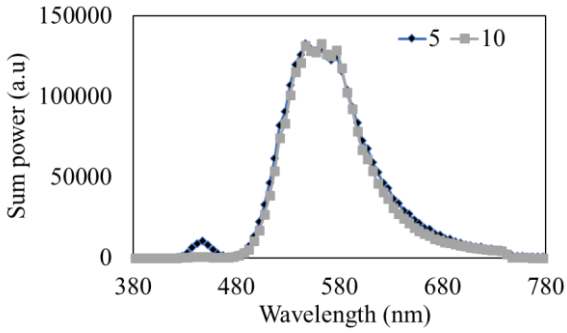

Figure 2. The discharge spectra for 6500 K WLED devices correlating with (Ba,Ca)ScO2F:Bi3+,K+concentration

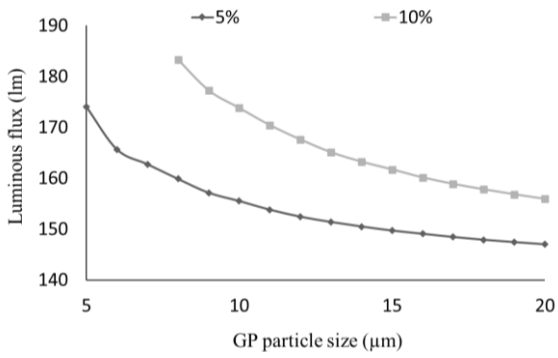

Figure 3. The luminous flux in WLED device correlating with (Ba,Ca)$ScO_2F:Bi^{3+},K^+$ dosage

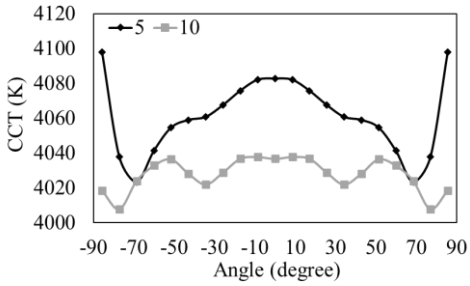

Figure 4. Relation between CCT for WLED device and (Ba,Ca)$ScO_2F:Bi^{3+},K^+$ concentration

Hue consistency is simply a factor used for examining hue output in WLED devices. It is impossible to say that hue quality is good when the hue homogeneity index is high. Hence, it is necessary to utilize CRI and color quality scale (CQS). The hue rendering index shows an object's actual hue when it is lit by illumination. If green illumination becomes excessive among the key chromas (green, blue, yellow), there will be an imbalance in hue gamut, altering the color precision in devices and yielding lesser chroma quality. Figure 5 exhibits one slight drop for CRI with (Ba,Ca)$ScO_2F:Bi^{3+},K^+$ sheet. The disadvantages would be minimal nevertheless since CRI would be only a flaw in CQS. CQS is formed through several factors: the first is CRI, the second is watchers' taste, and the third is hue coordinate [28], [29]. CQS would be virtually an effective evaluation method when it comes to chroma efficiency. Judging Figure 6, CQS gets augmented using the distant (Ba,Ca)$ScO_2F:Bi^{3+},K^+$ sheet. On the other hand, the (Ba,Ca)$ScO_2F:Bi^{3+},K^+$ dosage would mostly leave CQS intact when the dosage is less than 10% wt. The substantial hue loss when green is prevalent results in CRI as well as CQS to be highly reduced with (Ba,Ca)$ScO_2F:Bi^{3+},K^+$ dosages exceeding 10% wt. For this reason, determining a compatible dosage is a must.

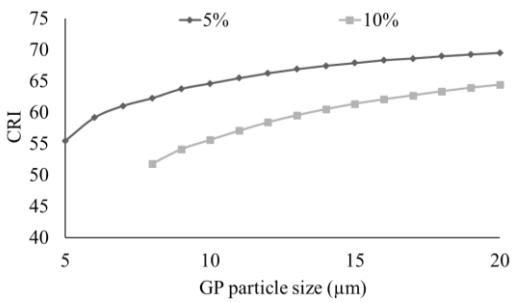

Figure 5. Relation between CRI for WLED device and (Ba,Ca)ScO2F:Bi3+,K+ dosage

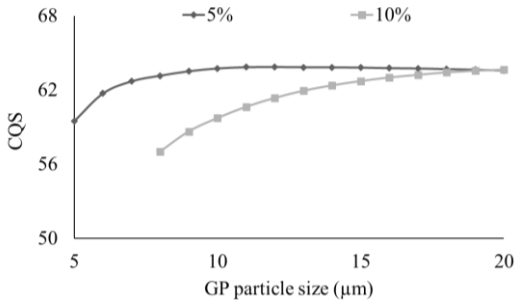

Figure 6. Relation between CQS for WLED device and (Ba,Ca)ScO2F:Bi3+,K+ dosage

4. CONCLUSION

The study shows how a dual-layer phosphorus arrangement's optical characteristics are affected by $(Ba,Ca)ScO_2F:Bi^{3+},K^+$ green phosphorus. Using Monte Carlo computer simulations, the study proved that $(Ba,Ca)ScO_2F:Bi^{3+},K^+$ is a suitable remedy for enhancing color consistency. This would be relevant if we employ WLED apparatuses with chroma temperature exceeding 8500 K along with ones with a hue color temperature of 5600 K. As a result, the results from said inquiry have succeeded in increasing color quality and luminous flux, which was a challenging task given the dispersed arrangement of phosphorus. CRI and CQS do yield one little downside, though. The CRI and CQS drastically decrease when the concentration of $(Ba,Ca)ScO_2F:Bi^{3+},K^+$ is raised to excessive levels. Subsequently, determining the proper concentration by considering the objectives of the producer. The study has offered beneficial information for creating WLEDs with improved color uniformity and luminous flux.

REFERENCES

[1] J. Ji, G. Zhang, S. Yang, X. Feng, X. Zhang, and C. C. Yang, "Theoretical analysis of a white-light LED array based on a GaN nanorod structure," *Applied Optics*, vol. 59, no. 8, p. 2345, Mar. 2020, doi: 10.1364/ao.387059.

[2] F. Hu *et al.*, "Si-substrate LEDs with multiple superlattice interlayers for beyond 24 Gbps visible light communication," *Photonics Research*, vol. 9, no. 8, p. 1581, Aug. 2021, doi: 10.1364/prj.424934.

[3] L. Y. Kuritzky, C. Weisbuch, and J. S. Speck, "Prospects for 100% wall-plug efficient III-nitride LEDs," *Optics Express*, vol. 26, no. 13, p. 16600, Jun. 2018, doi: 10.1364/oe.26.016600.

[4] M. M. Muhammed, J. Xu, N. Wehbe, and I. S. Roqan, " Carrier dynamics of In x Ga 1-x N/GaN multiple quantum wells grown on (−201) β-Ga 2 O 3 for bright vertical light emitting diodes ," *Optics Express*, vol. 26, no. 12, p. 14869, Jun. 2018, doi: 10.1364/oe.26.014869.

[5] Y. Li *et al.*, "48 × 48 pixelated addressable full-color micro display based on flip-chip micro LEDs," *Applied Optics*, vol. 58, no. 31, p. 8383, Nov. 2019, doi: 10.1364/ao.58.008383.

[6] L. Lin *et al.*, "InGaN/GaN ultraviolet LED with a graphene/AZO transparent current spreading layer," *Optical Materials Express*, vol. 8, no. 7, p. 1818, Jul. 2018, doi: 10.1364/ome.8.001818.

[7] S. Hussain *et al.*, "Stable and high performance all-inorganic perovskite light-emitting diodes with anti-solvent treatment," *Chinese Optics Letters*, vol. 19, no. 3, p. 030005, 2021, doi: 10.3788/col202119.030005.

[8] J. H. Lee, S. G. Han, and M. J. Jin, "Minimum achievable height of a single-module LED low-beam projection headlamp," *Applied Optics*, vol. 60, no. 20, p. E8, Jul. 2021, doi: 10.1364/ao.417144.

[9] N. Susilo *et al.*, "Improved performance of UVC-LEDs by combination of high-temperature annealing and epitaxially laterally overgrown AlN/sapphire," *Photonics Research*, vol. 8, no. 4, p. 589, Apr. 2020, doi: 10.1364/prj.385275.

[10] L. Huang, S. Wen, Z. Yan, H. Song, S. Su, and W. Guan, "Single LED positioning scheme based on angle sensors in robotics," *Applied Optics*, vol. 60, no. 21, p. 6275, Jul. 2021, doi: 10.1364/ao.425744.

[11] L.-C. Lai, D.-J. Lin, W.-H. Chiang, C.-T. Huang, G.-R. Lin, and J.-J. Huang, "Beyond GHz optical frequency up-converted modulation of LEDs with integrated acousto-optic transducer," *Optics Letters*, vol. 46, no. 20, p. 5189, Oct. 2021, doi: 10.1364/ol.440983.

[12] J. Guo, J. Zhang, Y. Zhang, and G. Xin, "Efficient multi-LED dimming control scheme with space–time codes for VLC systems," *Applied Optics*, vol. 59, no. 28, p. 8553, Oct. 2020, doi: 10.1364/ao.399313.

[13] W. Tian, L. Dou, Z. Jin, J. Xiao, and J. Li, "Full-color micro-LED displays with cadmium-free quantum dots patterned by photolithography technology," *Applied Optics*, vol. 59, no. 35, p. 11112, Dec. 2020, doi: 10.1364/ao.412267.

[14] Y. Zhang *et al.*, "Full wafer scale electroluminescence properties of AlGaN-based deep ultraviolet LEDs with different well widths," *Optics Letters*, vol. 46, no. 9, p. 2111, May 2021, doi: 10.1364/ol.423264.

[15] J. H. Lee, A. B. M. H. Islam, T. K. Kim, Y.-J. Cha, and J. S. Kwak, "Impact of tin-oxide nanoparticles on improving the carrier transport in the Ag/p-GaN interface of InGaN/GaN micro-light-emitting diodes by originating inhomogeneous Schottky barrier height," *Photonics Research*, vol. 8, no. 6, p. 1049, Jun. 2020, doi: 10.1364/prj.385249.

[16] R. T. Velpula, B. Jain, S. Velpula, H.-D. Nguyen, and H. P. T. Nguyen, "High-performance electron-blocking-layer-free deep ultraviolet light-emitting diodes implementing a strip-in-a-barrier structure," *Optics Letters*, vol. 45, no. 18, p. 5125, Sep. 2020, doi: 10.1364/ol.400917.

[17] B. Romeira, J. Borme, H. Fonseca, J. Gaspar, and J. B. Nieder, "Efficient light extraction in subwavelength GaAs/AlGaAs nanopillars for nanoscale light-emitting devices," *Optics Express*, vol. 28, no. 22, p. 32302, Oct. 2020, doi: 10.1364/oe.402887.

[18] S. Lan, B. Tang, H. Hu, and S. Zhou, "Strategically constructed patterned sapphire with silica array to boost substrate performance in GaN-based flip-chip visible light-emitting diodes," *Optics Express*, vol. 28, no. 25, p. 38444, Dec. 2020, doi: 10.1364/oe.413088.

[19] B. Jain *et al.*, "High performance electron blocking layer-free InGaN/GaN nanowire white-light-emitting diodes," *Optics Express*, vol. 28, no. 1, p. 665, Jan. 2020, doi: 10.1364/oe.28.000665.

[20] Z. Zhuang, D. Iida, P. Kirilenko, and K. Ohkawa, "Improved performance of InGaN-based red light-emitting diodes by micro-hole arrays," *Optics Express*, vol. 29, no. 19, p. 29780, Sep. 2021, doi: 10.1364/oe.435556.

[21] S. Bharadwaj *et al.*, "Enhanced injection efficiency and light output in bottom tunnel-junction light-emitting diodes," *Optics Express*, vol. 28, no. 4, p. 4489, Feb. 2020, doi: 10.1364/oe.384021.

[22] A. Pandey, W. J. Shin, X. Liu, and Z. Mi, "Effect of electron blocking layer on the efficiency of AlGaN mid-ultraviolet light emitting diodes," *Optics Express*, vol. 27, no. 12, p. A738, Jun. 2019, doi: 10.1364/oe.27.00a738.

[23] S. Zhou, X. Liu, H. Yan, Z. Chen, Y. Liu, and S. Liu, "Highly efficient GaN-based high-power flip-chip light-emitting diodes," *Optics Express*, vol. 27, no. 12, p. A669, Jun. 2019, doi: 10.1364/oe.27.00a669.

[24] E. Chen *et al.*, "Edge/direct-lit hybrid mini-LED backlight with U-grooved light guiding plates for local dimming," *Optics Express*, vol. 29, no. 8, p. 12179, Apr. 2021, doi: 10.1364/oe.421346.

[25] Y. Zhou, J. Wu, J. Suo, X. Han, G. Zheng, and Q. Dai, "Single-shot lensless imaging via simultaneous multi-angle LED illumination," *Optics Express*, vol. 26, no. 17, p. 21418, Aug. 2018, doi: 10.1364/oe.26.021418.

[26] M. Chlipala *et al.*, "Nitride light-emitting diodes for cryogenic temperatures," *Optics Express*, vol. 28, no. 20, p. 30299, Sep. 2020, doi: 10.1364/OE.403906.

[27] A. Zhang *et al.*, "Enhanced amplified spontaneous emission from conjugated light-emitting polymer integrated with silicon nitride grating structures," *OSA Continuum*, vol. 2, no. 10, p. 2875, Oct. 2019, doi: 10.1364/osac.2.002875.
[28] K. Tian *et al.*, "On the polarization self-screening effect in multiple quantum wells for nitride-based near ultraviolet light-emitting diodes," *Chinese Optics Letters*, vol. 17, no. 12, p. 122301, 2019, doi: 10.3788/col201917.122301.
[29] A. Hassan, S. Khan, K. Rasul, and A. Hussain, "Lensless on-chip LED array microscope using amplitude and phase masks," *Journal of the Optical Society of America B*, vol. 37, no. 12, p. 3652, Dec. 2020, doi: 10.1364/JOSAB.396076.

BIOGRAPHIES OF AUTHORS

Le Doan Duy received the Master degree in physics from Can Tho University, Vietnam. He is working as a lecturer at the Faculty of Basic Sciences, Vinh Long University of Technology Education, Vietnam. His research interests focus on developing the patterned substrate with micro- and nano-scale to apply for physical and chemical devices such as solar cells, OLED, photoanode, theory physics. He can be contacted at email: duyld@vlute.edu.vn.

My Hanh Nguyen Thi received a Bachelor of Physics from An Giang University, VietNam, Master of Theoretical Physics and Mathematical Physics, Hanoi National University of Education, VietNam. Currently, she is a lecturer at the Faculty of Mechanical Engineering, Industrial University of Ho Chi Minh City, Viet Nam. Her research interests are theoretical physics and mathematical physics. She can be contacted at email: nguyenthimyhanh@iuh.edu.vn.

Nguyen Le Thai received his BS in Electronic engineering from Danang University of Science and Technology, Vietnam, in 2003, MS in Electronic Engineering from Posts and Telecommunications Institute of Technology, Ho Chi Minh, Vietnam, in 2011 and PhD degree of Mechatronics Engineering from Kunming University of Science and Technology, China, in 2016. He is a currently with the Nguyen Tat Thanh University, Ho Chi Minh City, Vietnam. His research interests include the renewable energy, optimisation techniques, robust adaptive control, and signal processing. He can be contacted at email: nlthai@nttu.edu.vn.